# Abstracta

Ano XVIII - N. 03

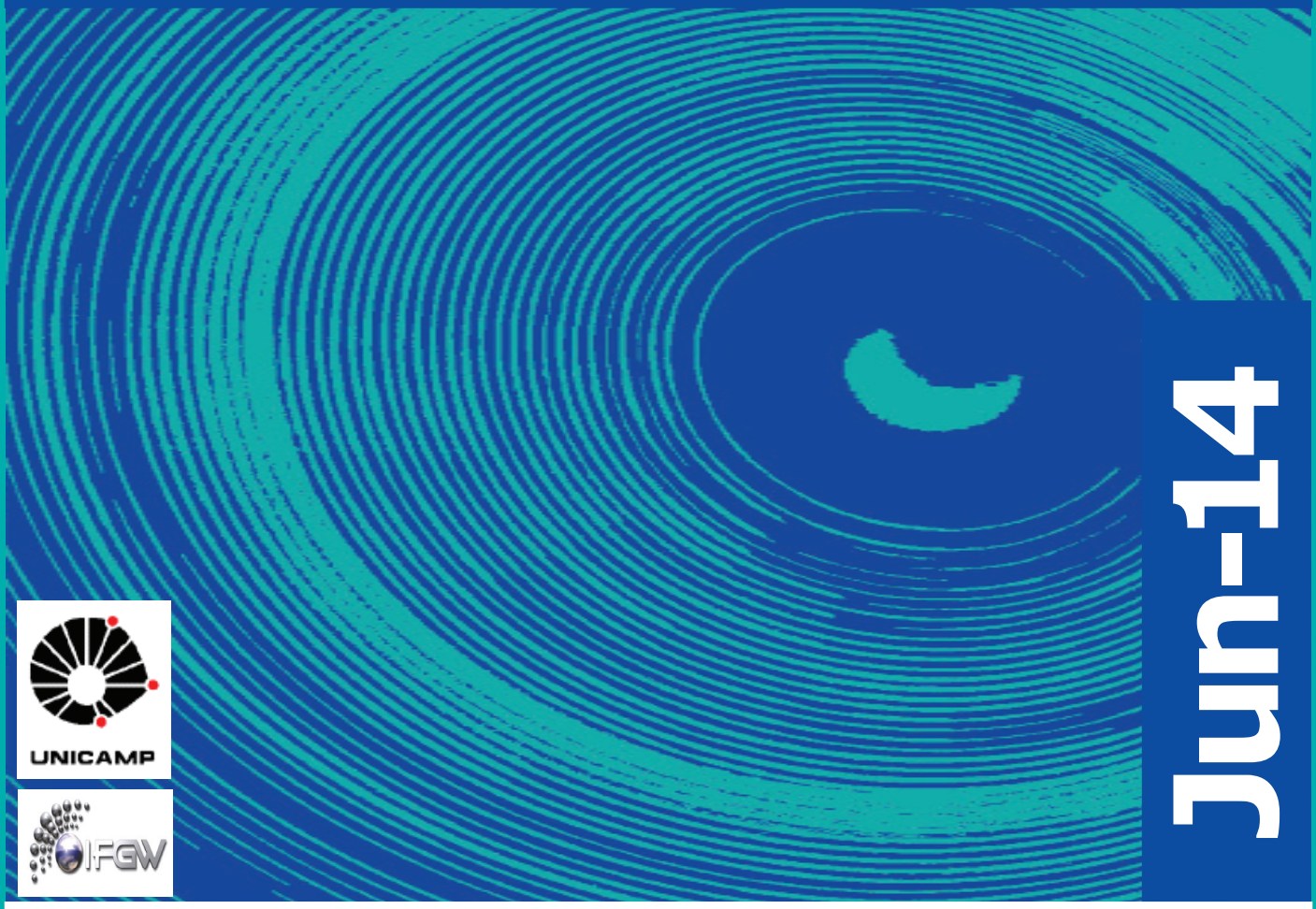

Jun-14

UNICAMP

IFGW

# Trabalhos Publicados

**[P123-2014] "A Simple Formula For The Third Integral Of Motion Of Disk-Crossing Stars In The Galaxy"**

**Vieira, Ronaldo S. S.***; Ramos-Caro, J.

We present a simple analytical formula for an approximated third integral of motion associated with nearly equatorial orbits in the Galaxy: I-3 = Z Sigma(1/3)(I) I, where Z(R) is the vertical amplitude of the orbit at galactocentric distance R and Sigma(I)(R) is the integrated dynamical surface mass density of the disk, a quantity which has recently become measurable. We also suggest that this relation is valid for disk-crossing orbits in a wide variety of axially symmetric galactic models, which range from razor-thin disks to disks with non-negligible thickness, whether or not the system includes bulges and halos. We apply our formalism to a Miyamoto-Nagai model and to a realistic model for the Milky Way. In both cases, the results provide fits for the shape of nearly equatorial orbits which are better than the corresponding curves obtained by the usual adiabatic approximation when the orbits have vertical amplitudes comparable to the disk's scale height. We also discuss the role of this approximate third integral of motion in modified theories of gravity.

**Astrophysical Journal 786[1], 27, 2014. DOI:** 10.1088/0004-637X/786/1/27

**[P124-2014] "Absence of exchange interaction between localized magnetic moments and conduction-electrons in diluted Er3+ gold-nanoparticles"**

**Lesseux, G. G.*; Iwamoto, W.***; Garcia-Flores, A. F.; **Urbano, R. R.*; Rettori, C.***

The Electron Spin Resonance (ESR) of diluted Er3+ magnetic ions in Au nanoparticles (NPs) is reported. The NPs were synthesized by reducing chloro triphenyl-phosphine gold(I) and erbium(III) trifluoroacetate. The Er3+ g-value along with the observed hyperfine splitting indicate that the Er3+ impurities are in a local cubic symmetry. Furthermore, the Er3+ ESR spectra show that the exchange interaction between the 4f and the conduction electrons (ce) is absent or negligible in Au1-xErx NPs, in contrast to the ESR results in bulk Au1-xErx. Therefore, the nature of this interaction needs to be reexamined at the nano scale range.

**Journal Of Applied Physics 115[17], 17E128, 2014. DOI:** 10.1063/1.4867126

**[P125-2014] "An All-Optical Ocdma Encoder With Simultaneous Signal Regeneration Based On Fiber Four-Wave Mixing"**

Galdino, L.; Abbade, M. L. F.; Bonani, L. H.; Marconi, J. D.; **Fragnito, H. L.***; Moschim, E.

A new all-optical optical code division multiple access encoder that simultaneously regenerates input signals is proposed and experimentally investigated. The device is based on a fiber four-wave mixing and experimental results show that eye penalties may be decreased up to 5.1 dB.

**Microwave And Optical Technology Letters 56[5], 1024-1028, 2014. DOI:** 10.1002/mop.28263

**[P126-2014] "Bipartite bound entanglement in continuous variables through degaussification"**

**Steinhoff, F. E. S.*; de Oliveira, M. C.***; Sperling, J.; Vogel, W.

We introduce a class of bipartite entangled continuous variable states that are positive under a partial transposition (PPT) operation, i.e., PPT bound entangled. These states are based on realistic preparation procedures in optical systems, being thus a feasible option to generate and observe genuinely bipartite bound entanglement in high precision experiments. One fundamental step in our scheme is to perform a non-Gaussian operation over a single-mode Gaussian state. This degaussification procedure is achieved through a modified single-photon addition, which is a procedure that is currently being investigated in diverse optical setups. Although dependent on a single-photon detection in an idler channel, the preparation can be made unconditional after a calibration of the apparatus. The detection and proof of bound entanglement is made by means of the range criterion, theory of Hankel operators and Gerschgorin Disk's perturbation theorems.

**Physical Review A 89[3], 032313, 2014. DOI:** 10.1103/PhysRevA.89.032313

**[P127-2014] "Bond length and electric current oscillation of long linear carbon chains: Density functional theory, MpB model, and quantum spin transport studies"**

**Oeiras, R. Y.*; da Silva, E. Z.***

Carbon linear atomic chains attached to graphene have experimentally been produced. Motivated by these results, we study the nature of the carbon bonds in these nanowires and how it affects their electrical properties. In the present study we investigate chains with different numbers of atoms and we observe that nanowires with odd number of atoms present a distinct behavior than the ones with even numbers. Using graphene nanoribbons as leads, we identify differences in the quantum transport of the chains with the consequence that even and odd numbered chains have low and high electrical conduction, respectively. We also noted a dependence of current with the wire size. We study this unexpected behavior using a combination of first principles calculations and simple models based on chemical bond theory. From our studies, the electrons of carbon nanowires present a quasi-free electron behavior and this explains qualitatively the high electrical conduction and the bond lengths with unexpected values for the case of odd nanowires. Our study also allows the understanding of the electric conduction dependence with the number of atoms and their parity in the chain. In the case of odd number chains a proposed pi-bond (MpB) model describes unsaturated carbons that introduce a mobile pi-bond that changes dramatically the structure and transport properties of these wires. Our results indicate that the nature of bonds plays the main role in the oscillation of quantum electrical conduction for chains with even and odd number of atoms and also that nanowires bonded to graphene nanoribbons behave as a quasi-free electron system, suggesting that this behavior is general and it could also remain if the chains are bonded to other materials.

**Journal Of Chemical Physics 140[13], 134703, 2014. DOI:** 10.1063/1.4869858

**[P128-2014] "Characterisation of a Nafion film by optical fibre Fabry-Perot interferometry for humidity sensing"**

Santos, J. S.; Raimundo, I. M.; **Cordeiro, C. M. B.*; Biazoli, C. R.***; Gouveia, C. A. J.; Jorge, P. A. S.

Nafion has been evaluated as a sensing phase of an optical fibre humidity sensor based on a low-finesse Fabry-Perot interferometer. The sensor was constructed by manual deposition of a drop of a Nafion solution on the tip of a single mode optical fibre, forming a Fabry-Perot resonant cavity. The absorption of water by the Nafion film makes it swells, changing its refractive index and the length of the cavity, which produces a phase shift in the interference signal.

The sensitivity, stability and response time of the sensor were evaluated in the RH range from 22 to 80% by analysing the correspondent reflection spectra of the interference fringes. As a result, it was obtained that Nafion can be used as sensing phase of an optical fibre humidity sensor based on optical fibre Fabry-Perot interferometry, presenting a response time of 242 ms (3% RH variation) and a sensitivity of 3.5 nm/%RH.

**Sensors And Actuators B-Chemical 196, 99-105, 2014. DOI:** 10.1016/j.snb.2014.01.101

**[P129-2014] "Combined Analysis of nu(mu) Disappearance and nu(mu) -> nu(e) Appearance in MINOS Using Accelerator and Atmospheric Neutrinos"**

Adamson, P.; Anghel, I.; Aurisano, A.; **Coelho, J. A. B.*; Escobar, C. O.*** ; et al.
MINOS Collaboration

We report on a new analysis of neutrino oscillations in MINOS using the complete set of accelerator and atmospheric data. The analysis combines the nu(mu) disappearance and nu(e) appearance data using the three-flavor formalism. We measure vertical bar Delta m(32)(2)vertical bar = [2.28-2.46] x 10(-3) eV(2) (68% C.L.) and sin(2)theta(23) = 0.35-0.65 (90% C.L.) in the normal hierarchy, and vertical bar Delta m(32)(2)vertical bar = [2.32-2.53] x 10(-3) eV(2) (68% C.L.) and sin(2)theta(23) = 0.34-0.67 (90% C.L.) in the inverted hierarchy. The data also constrain delta(CP), the theta(23) octant degeneracy and the mass hierarchy; we disfavor 36% (11%) of this three-parameter space at 68% (90%) C.L.

**Physical Review Letters 112[19], 191801, 2014. DOI:** 10.1103/PhysRevLett.112.191801

**[P130-2014] "Defect spectroscopy of single ZnO microwires"**

Villafuerte, M.; Ferreyra, J. M.; Zapata, C.; Barzola-Quiquia, J.; **Iikawa, F.***; Esquinazi, P.; Heluani, S. P.; de Lima, M. M.; Cantarero, A.

The point defects of single ZnO microwires grown by carbothermal reduction were studied by microphotoluminescence, photoresistance excitation spectra, and resistance as a function of the temperature. We found the deep level defect density profile along the microwire showing that the concentration of defects decreases from the base to the tip of the microwires and this effect correlates with a band gap narrowing. The results show a characteristic deep defect levels inside the gap at 0.88 eV from the top of the VB. The resistance as a function of the temperature shows defect levels next to the bottom of the CB at 110 meV and a mean defect concentration of 4 x 10(18) cm(-3). This combination of techniques allows us to study the band gap values and defects states inside the gap in single ZnO microwires and opens the possibility to be used as a defect spectroscopy method

**Journal Of Applied Physics 115[13], 133101, 2014. DOI:** 10.1063/1.4869555

**[P131-2014] "Development of a quartz tuning-fork-based force sensor for measurements in the tens of nanoNewton force range during nanomanipulation experiments"**

**Oiko, V. T. A.***; Martins, B. V. C.; Silva, P. C.; **Rodrigues, V.*; Ugarte, D.***

Understanding the mechanical properties of nanoscale systems requires new experimental and theoretical tools. In particular, force sensors compatible with nanomechanical testing experiments and with sensitivity in the nN range are required. Here, we report the development and testing of a tuning-fork-based force sensor for in situ nanomanipulation experiments inside a scanning electron microscope. The sensor uses a very simple design for the electronics and it allows the direct and quantitative force measurement in the 1-100 nN force range. The sensor response is initially calibrated against a nN range force standard, as, for example, a calibrated Atomic Force Microscopy cantilever; subsequently, applied force values can be directly derived using only the electric signals generated by the tuning fork. Using a homemade nanomanipulator, the quantitative force sensor has been used to analyze the mechanical deformation of multi-walled carbon nanotube bundles, where we analyzed forces in the 5-40 nN range, measured with an error bar of a few nN.

**Review Of Scientific Instruments 85[3], 035003, 2014. DOI:** 10.1063/1.4868236

**[P132-2014] "Deviations from reversible dynamics in a qubit-oscillator system coupled to a very small environment"**

**Vidiella-Barranco, A.***

In this contribution it is considered a simple and solvable model consisting of a qubit in interaction with an oscillator exposed to a very small "environment" (a second qubit). An isolated qubit-oscillator system having the oscillator initially in one of its energy eigen-states exhibits Rabi oscillations, an evidence of coherent quantum behaviour. It is shown here in which way the coupling to a small "environment" disrupts such regular behaviour, leading to a quasi-periodic dynamics for the qubit linear entropy. In particular, it is found that the linear entropy is very sensitive to the amount of mixedness of the "environment". For completeness, fluctuations in the oscillator energy are also taken into account.

**Physica a-Statistical Mechanics and Its Applications 402, 209-215, 2014. DOI:** 10.1016/j.physa.2014.02.004

**[P133-2014] "Disorder in quantum critical superconductors"**

Seo, S.; Xin Lu, J-X. Zhu, **Urbano, R. R.***; Curro, N.; Bauer, E. D.; Sidorov, V. A.; Pham, L. D.; Tuson Park, Fisk, Z.; Thompson, J. D.

In four classes of materials—the layered copper oxides, organics, iron pnictides and heavy-fermion compounds—an unconventional superconducting state emerges as a magnetic transition is tuned towards absolute zero temperature, that is, towards a magnetic quantum critical point1 (QCP). In most materials, the QCP is accessed by chemical substitution or applied pressure. CeCoIn5 is one of the few materials that are 'born' as a quantum critical superconductor2, 3, 4 and, therefore, offers the opportunity to explore the consequences of chemical disorder. Cadmium-doped crystals of CeCoIn5 are a particularly interesting case where Cd substitution induces long-range magnetic order5, as in Zn-doped copper oxides6, 7. Applied pressure globally suppresses the Cd-induced magnetic order and restores bulk superconductivity. Here we show, however, that local magnetic correlations, whose spatial extent decreases with applied pressure, persist at the extrapolated QCP. The residual droplets of impurity-induced magnetic moments prevent the reappearance of conventional signatures of quantum criticality, but induce a heterogeneous electronic state. These discoveries show that spin droplets can be a source of electronic heterogeneity and emphasize the need for caution when interpreting the effects of tuning a correlated system by chemical substitution.

**Nature Physics 10, 120-125, 2014. DOI:** 10.1038/nphys2820
**(Artigo destaque de capa)**

**[P134-2014] "Effects of divergent ghost loops on the Green's functions of QCD"**

**Aguilar, A. C.***; Binosi, D.; Ibanez, D.; Papavassiliou, J.

In the present work, we discuss certain characteristic features encoded in some of the fundamental QCD Green's functions, for which the origin can be traced back to the nonperturbative masslessness of the ghost field, in the Landau gauge. Specifically, the ghost loops that contribute to these Green's functions display infrared divergences, akin to those encountered in the perturbative treatment, in contradistinction to the gluonic loops, for which perturbative divergences are tamed by the dynamical generation of an effective gluon mass. In d = 4, the aforementioned divergences are logarithmic, thus causing a relatively mild impact, whereas in d = 3 they are linear, giving rise to enhanced effects. In the case of the gluon propagator, these effects do not interfere with its finiteness, but make its first derivative diverge at the origin, and introduce a maximum in the region of infrared momenta. The three-gluon vertex is also affected, and the induced divergent behavior is clearly exposed in certain special kinematic configurations, usually considered in lattice simulations; the sign of the corresponding divergence is unambiguously determined. The main underlying concepts are developed in the context of a simple toy model, which demonstrates clearly the interconnected nature of the various effects. The picture that emerges is subsequently corroborated by a detailed nonperturbative analysis, combining lattice results with the dynamical integral equations governing the relevant ingredients, such as the nonperturbative ghost loop and the momentumdependent gluon mass.

**Physical Review D 89[8], 085008, 2014. DOI:** 10.1103/PhysRevD.89.085008

**[P135-2014] "Elastic scattering of slow electrons by n-pentanol alcohol"**

**de Oliveira, E. M.***; Varella, M. T. do N.; Bettega, M. H. F.; **Lima, M. A. P.***

We report elastic integral (ICS), differential (DCS) and momentum transfer cross sections (MTCS) for low-energy electron scattering by n-pentanol alcohol in the gas phase. The Schwinger multichannel method implemented with pseudopotentials was employed in the calculations. The DCSs were computed for energies from 1 to 50 eV and the ICS and MTCS from 1 to 100 eV. Due to the significant value of the electric dipole moment, the DCSs are dominated by strong forward scattering. Despite this fact, the DCS around 10 eV displays a behavior related to a f-wave scattering pattern at intermediate angles which may be associated with shape resonances. This result is consistent with the ICS and the MTCS since they show a pronounced peak near this energy. For energies below 1 eV, the MTCS obtained in the static-exchange plus polarization approximation does not increase, as expected for polar molecules, suggesting that a Ramsauer-Townsend minimum could be present. This finding motivated us to revisit the previously studied methanol, ethanol, n-propanol and n-butanol molecules and to perform new calculations for impact energies below 1 eV (not addressed before). With the inclusion of polarization effects, the MTCS for the five alcohols suggest a Ramsauer-Townsend minimum coming from the negative to the positive scattering energies. To the best of our knowledge, there are neither experimental nor calculated cross sections for comparison with the present results.

**European Physical Journal D 68[3], 65, 2014. DOI:** 10.1140/epjd/e2014-40680-y

**[P136-2014] "Embedded coupled microrings with high-finesse and close-spaced resonances for optical signal processing"**

**Souza, M. C. M. M.*; Barea, L. A. M.*; Vallini, F.*; Rezende, G. F. M.*; Wiederhecker, G. S.*; Frateschi, N. C.***

Single microring resonators have been used in applications such as wavelength multicasting and microwave photonics, but the dependence of the free spectral range with ring radius imposes a trade-off between the required GHz optical channel spacing, footprint and power consumption. We demonstrate four-channel all-optical wavelength multicasting using only 1 mW of control power, with converted channel spacing of 40-60 GHz. Our device is based on a compact embedded microring design fabricated on a scalable SOI platform. The coexistence of close resonance spacing and high finesse (205) in a compact footprint is possible due to enhanced quality factors (30,000) resulting from the embedded configuration and the coupling--strength dependence of resonance spacing, instead of ring size. In addition, we discuss the possibility of achieving continuously mode splitting from a single-notch resonance up to 40 GHz.

**Optics Express 22[9], 10430-10438, 2014. DOI:** 10.1364/OE.22.010430

**[P137-2014] "Event activity dependence of (nS) production in=5.02 TeV pPb and=2.76 TeV pp collisions"**

Chatrchyan, S.; Khachatryan, V.; Sirunyan, A. M.; **Chinellato, J.*; Tonelli Manganote, E. J.***; et al.
CMS Collaboration

The production of (1S), (2S), and (3S) is investigated in pPb and pp collisions at centre-of-mass energies per nucleon pair of 5.02 TeV and 2.76 TeV, respectively. The datasets correspond to integrated luminosities of about 31 nb(-1) (pPb) and 5.4 pb(-1) (pp), collected in 2013 by the CMS experiment at the LHC. Upsilons that decay into muons are reconstructed within the rapidity interval |y (CM)| < 1.93 in the nucleon-nucleon centre--of-mass frame. Their production is studied as a function of two measures of event activity, namely the charged-particle multiplicity measured in the pseudorapidity interval |eta| < 2.4, and the sum of transverse energy deposited at forward pseudorapidity, 4.0 < |eta| < 5.2. The cross sections normalized by their event activity integrated values, (nS)/aEuro(nS) aEuro parts per thousand, are found to rise with both measures of the event activity in pp and pPb. In both collision systems, the ratios of the excited to the ground state cross sections, (nS)/ (1S), are found to decrease with the charged-particle multiplicity, while as a function of the transverse energy the variation is less pronounced. The event activity integrated double ratios, [(nS)/ (1S)](pPb) /[(nS)/ (1S)](pp), are also measured and found to be 0.83 +/- 0.05 (stat.) +/- 0.05 (syst.) and 0.71 +/- 0.08 (stat.) +/- 0.09 (syst.) for (2S) and (3S), respectively.

**Journal Of High Energy Physics 4, 103, 2014. DOI:** 10.1007/JHEP04(2014)103

**[P138-2014] "Event-plane-dependent dihadron correlations with harmonic v(n) subtraction in Au plus Au collisions at v root sNN=200 GeV"**

Agakishiev, H.; Aggarwal, M. M.; Ahammed, Z.; Brandin, A. V.; **Derradi de Souza, R.*; Takahashi, J.*; Vasconcelos, G. M. S.* ; et al.**
STAR Collaboration

STAR measurements of dihadron azimuthal correlations (Lambda phi) are reported in midcentral (20-60%) Au + Au collisions at v root sNN = 200 GeV as a function of the trigger particle's azimuthal angle relative to the event plane, phi(s) = | phi(1) -psi(EP)|. The elliptic (v(2)), triangular (v(3)), and quadratic (v(4)) flow harmonic backgrounds are subtracted using the zero yield at mini + Au collisions. It is found that a finite near-side (| Delta phi | < pi/2) long-range pseudorapidity correlation (ridge) is present in the in-plane direction (phi(s) similar to 0).

The away-side (| Delta phi | > pi/2) correlation shows a modification from d+ Au data, varying with fs. The modification may be a consequence of path-length-dependent jet quenching and may lead to a better understanding of high-density QCD.

**Physical Review C 89[4], UNSP 041901, 2014. DOI:** 10.1103/PhysRevC.89.041901

**[P139-2014] "Evolution of the magnetic properties along the RCuBi2 (R=Ce, Pr, Nd, Gd, Sm) series of intermetallic compounds"**

**Jesus, C. B. R.*; Piva, M. M.*; Rosa, P. F. S.*; Adriano, C.*; Pagliuso, P. G.***

In this paper, the evolution of the magnetic properties along the series of intermetallic compounds RCuBi2 (R Ce, Pr, Nd, Gd, Sm) is discussed. These compounds crystallize in a tetragonal ZrCuSi2 (P4/nmm) structure, and our single crystals of RCuBi2 grown from Bi-flux show no evidence for Cu--deficiency [Ye et al., Acta Crystallogr. C 52, 1325 (1996)] as previously reported for R Ce. For R Ce, Pr, Gd, and Sm, we found an antiferromagnetic ordering at T-N similar to 16 K, 4.2 K, 13.6 K, and 4.9 K, respectively. For R Nd, we saw no evidence for a magnetic phase transition down to T = 2K. These values of TN clearly show a dramatic breakdown of the De Gennes factor in this series. We discuss our data taken into account the tetragonal crystalline electrical field and the anisotropic Ruderman-Kittel-Kasuya-Yoshida magnetic interaction between the R-ions in this family of compounds.

**Journal Of Applied Physics 115[17], 17E115, 2014. DOI:** 10.1063/1.4860657

**[P140-2014] "Gastro-Resistant Controlled Release of OTC Encapsulated in Alginate/Chitosan Matrix Coated with Acryl-EZE (R) MP in Fluidized Bed"**

Kleinubing, S. A.; Seraphim, D. C.; Vieira, M. G. A.; Canevesi, R. L. S.; da Silva, E. A.; **Cesar, C. L.***; Mei, L. H. I.

A gastro-resistant system of acryl-EZE (R) MP coated alginate/chitosan microparticles was developed to improve the controlled release of oxytetracycline (OTC). Microparticles were obtained by complex coacervation and, thereafter, were coated using fluidized polymer dispersion with acryl-EZE (R) MP solution. OTC distribution inside the microparticles was determined by multiphoton confocal microscopy, demonstrating the efficiency of encapsulation process. In vitro OTC release kinetic was performed in order to obtain the release profile in gastric and intestinal simulated fluids. A fast initial release, or burst effect, was observed with uncoated microparticles loaded with OTC in gastric conditions. When a 50% mass increase in acryl-EZE (R) MP coating was achieved, OTC release in acidic medium was greatly reduced, resulting in the expected gastro-resistant effect. Different mathematical models were applied to describe the drug diffusion across the polymer matrix. The Logistic model was the best tool to interpret the experimental data in most of the systems studied.

**Journal Of Applied Polymer Science 131[12], 40444, 2014. DOI:** 10.1002/app.40444

**[P141-2014] "Gd3+ spin-lattice relaxation via multi-band conduction electrons in Y1-xGdxIn3: an electron spin resonance study"**

Cabrera-Baez, M.; **Iwamoto, W.*;** Magnavita, E. T.; Osorio--Guillen, J. M.; Ribeiro, R. A.; Avila, M. A.; **Rettori, C.***

Interest in the electronic structure of the intermetallic compound YIn3 has been renewed with the recent discovery of superconductivity at T similar to 1 K, which may be filamentary in nature. In this work we perform electron spin resonance (ESR) experiments on Gd3+ doped YIn3 (Y1-xGdxIn3; 0.001 less than or similar to x <= 0.08), showing that the spin--lattice relaxation of the Gd3+ ions, due to the exchange interaction between the Gd3+ localized magnetic moment and the conduction electrons (ce), is processed via the presence of s-, p- and d-type ce at the YIn3 Fermi level. These findings are revealed by the Gd3+ concentration dependence of the Korringa-like relaxation rate d(Delta H)/dT and g-shift (Delta g = g - 1.993), that display bottleneck relaxation behavior for the s- electrons and unbottleneck behavior for the p- and d--electrons. The Korringa- like relaxation rates vary from 22(2) Oe/K for x. 0.001 to 8(2) Oe/K for x = 0.08 and the g- shift values change, respectively, from a positive.g = + 0.047(10) to a negative Delta g = - 0.008( 4). Analysis in terms of a three-band ce model allows the extraction of the corresponding exchange interaction parameters J(fs), J(fp) and J(fd).

**Journal Of Physics-Condensed Matter 26[17], 175501, 2014. DOI:** 10.1088/0953-8984/26/17/175501

**[P142-2014] "High field nuclear magnetic resonance in transition metal substituted BaFe2As2"**

**Garitezi, T. M.*; Lesseux, G. G.*; Rosa, P. F. S.*; Adriano, C.***; Reyes, A. P.; Kuhns, P. L.; **Pagliuso, P. G.*; Urbano, R. R.***

We report high field As-75 nuclear magnetic resonance (NMR) measurements on Co and Cu substituted BaFe2As2 single crystals displaying same structural/magnetic transition T-0 similar or equal to 128 K. From our anisotropy studies in the paramagnetic state, we strikingly found virtually identical quadrupolar splitting and consequently the quadrupole frequency nu(Q) similar or equal to 2: 57(1) MHz for both compounds, despite the claim that each Cu delivers 2 extra 3d electrons in BaFe-2As2 compared to Co substitution. These results allow us to conclude that a subtle change in the crystallographic structure, particularly in the Fe-As tetrahedra, must be the most probable tuning parameter to determine T-0 in this class of superconductors rather than electronic doping. Furthermore, our NMR data around T-0 suggest coexistence of tetragonal/paramagnetic and orthorhombic/antiferromagnetic phases between the structural and the spin density wave magnetic phase transitions, similarly to what was reported for K-doped BaFe2As2 [Urbano et al., Phys. Rev. Lett. 105, 107001 (2010)].

**Journal Of Applied Physics 115[17], 17D711, 2014. DOI:** 10.1063/1.4864442

**[P143-2014] "Holographic recording and characterization of photorefractive Bi2TeO5 crystals at 633 nm wavelength light"**

de Oliveira, I.; Carvalho, J. F.; Fabris, Z. V.; **Frejlich, J.***

We report on the holographic recording on photorefractive Bi-2TeO5 crystals using lambda = 633 nm wavelength light. We studied the behavior of this material under the action of this low photonic energy light and found out the presence of a fast and a slow hologram, both of photorefractive nature and exhibiting rather high diffraction efficiencies. The faster and the slower holograms are based on the excitation and diffusion of oppositely charged carriers (likely electrons and holes). Relevant parameters for the photoactive centers responsible for both kind of holograms were characterized using purely holographic techniques. No evidences of non-photosensitive ionic charge carriers being involved in the recording process at room temperature nor self-fixing effects were found.

**Journal Of Applied Physics 115[16], UNSP 163514, 2014. DOI:** 10.1063/1.4871807

**[P144-2014] "Ideal Shear Strength of a Quantum Crystal"**

**Borda, E. J. L.***; Cai, W.; **de Koning, M.***

Using path-integral Monte Carlo simulations, we compute the ideal shear strength (ISS) on the basal plane of hcp He-4. The failure mode upon reaching the ISS limit is characterized by the homogeneous nucleation of a stacking fault and it is found to be anisotropic, consistent with Schmid's law of resolved shear stress. Comparing the ISS of hcp He-4 to a large set of classical crystals shows that it closely fits the approximately universal modified Frenkel model of ideal strength. In addition to giving quantitative stress levels for the homogeneous nucleation of extended defects in hcp He-4, our findings lend support to assumptions in the literature that inherently classical models remain useful for the description of mechanical behavior in quantum crystals.

**Physical Review Letters 112[15], 155303, 2014. DOI:** 10.1103/PhysRevLett.112.155303 **(Artigo destaque dos Editores)**

**[P145-2014] "Inclusive search for a vector-like T quark with charge 2/3 in pp collisions at root s=8 TeV"**

Chatrchyan, S.; Khachatryan, V.; Sirunyan, A. M.; **Chinellato, J.*; Tonelli Manganote, E. J.***; et al.
CMS Collaboration

A search is performed for a massive new vector-like quark T, with charge 2/3, that is pair produced together with its antiparticle in proton-proton collisions. The data were collected by the CMS experiment at the Large Hadron Collider in 2012 at root s = 8 TeV and correspond to an integrated luminosity of 19.5 fb(-1). The T quark is assumed to decay into three different final states, bW, tZ, and tH. The search is carried out using events with at least one isolated lepton. No deviations from standard model expectations are observed, and lower limits are set on the T quark mass at 95% confidence level. The lower limit lies between 687 and 782 GeV for all possible values of the branching fractions into the three different final states assuming strong production. These limits are the most stringent constraints to date on the existence of such a quark.

**Physics Letters B 729, 149-171, 2014. DOI:** 10.1016/j.physletb.2014.01.006

**[P146-2014] "(Invited) Rare Earth Luminescence in Nanostructured Amorphous Silicon Alloys"**

**Tessler, L. R.***

Rare Earth (RE) doped amorphous silicon alloys can be prepared by reactive RF sputtering from a Si target partially covered with metallic or oxide RE platelets using appropriate reactive atmospheres. We have studied Er3+, Nd3+, Eu3+and Tb3+ in a-Si:H, a-SiOx:H and a-SiNx:H. Annealing optimizes the photoluminescence and can induce the formation of Si nanocrystals. The RE act as nucleation centers. The RE ions present intense photoluminescence at room temperature. EXAFS measurements reveal a highly non-centrosymetric lattice site for Er in a-SiOx:H. This partially breaks the selection rule that forbids intra-4f transitions. The RE present two luminescence lifetimes, the fast component determined by the host and the slow component associated to the local symmetry ofthe ions. The amorphous and nanostructured hosts increase the cross section for RE excitation by a few orders of magnitude, making the materials practical for applications as phosphors and active amplifiers.

**ECS Transactions 61[5], 107-113, 2014. DOI:** 10.1149/06105.0107ecst

**[P147-2014] "Jet-Hadron Correlations in root s(NN)=200 GeV p plus p and Central Au plus Au Collisions"**

Adamczyk, L.; Adkins, J. K.; Agakishiev, G.; de Souza, R. **Derradi*; Takahashi, J.*; Vasconcelos, G. M. S.*** ; et al.
STAR Collaboration

Azimuthal angular correlations of charged hadrons with respect to the axis of a reconstructed (trigger) jet in Au + Au and p + p collisions at root s(NN) = 200 GeV in STAR are presented. The trigger jet population in Au + Au collisions is biased toward jets that have not interacted with the medium, allowing easier matching of jet energies between Au + Au and p + p collisions while enhancing medium effects on the recoil jet. The associated hadron yield of the recoil jet is significantly suppressed at high transverse momentum (p(T)(assoc)) and enhanced at low p(T)(assoc) in 0%-20% central Au + Au collisions compared to p + p collisions, which is indicative of medium-induced parton energy loss in ultrarelativistic heavy-ion collisions.

**Physical Review Letters 112[12], 122301, 2014. DOI:** 10.1103/PhysRevLett.112.122301

**[P148-2014] "Magnetizations and magneto-transport properties of Ni-doped PrFeO3 thin films"**

Mir, F. A.; **Sharma, S. K.***; Kumar, R.

The present study reports the magnetizations and magneto--transport properties of PrFe1-xNixO3 thin films grown by pulsed laser ablation technique on LaAlO3 substrates. From DC M/H plots of these films, weak ferromagnetism or ferrimagnetism behaviors are observed. With Ni substitution, reduction in saturation magnetization is also seen. With Ni doping, variations in saturation field (H-s), coercive field (H-c), Weiss temperature (q), and effective magnetic moment (p(eff)) are seen. A small change of magnetoresitance with application of higher field is observed. Various essential parameters like density of state (N-f) at Fermi level, Mott's characteristic temperature (T-0), and activation energy (E-a) in the presence of and in the absence of magnetic field are calculated. The present observed magnetic properties are related to the change of Fe-O bond length (causing an overlap between the oxygen p orbital and iron d orbital) and the deviation of the Fe-O--Fe angle from 180 degrees. Reduction of magnetic domain after Ni doping is also explored to explain the present observed magnetic behavior of the system. The influence of doping on various transport properties in these thin films indicates a distortion in the lattice structure and single particle band width, owing to stress-induced reduction in unit cell volume.

**Chinese Physics B 23[4], 048101, 2014. DOI:** 10.1088/1674-1056/23/4/048101

**[P149-2014] "Magnetoelectric properties of laminated La0.7Ba0.3MnO3-BaTiO3 ceramic composites"**

Clabel, J. L. H.; Zabotto, F. L.; Nogueira, I. C.; Schio, P.; Garcia, D.; **de Lima, O. F.***; Leite, E. R.; Moreira, F. M. A.; Cardoso, C. A.

Multiferroic laminated ceramic composites consisting of piezoelectric (BaTiO3, phase B) magnetostrictive (La0.7Ba0.3MnO3, phase L) materials were synthesized by the Pechini method. The composites were sintered separately and in the form of L-B-L, in order to compare the properties of the separate phases and the laminated material.

X-ray diffraction analysis of the separate phases revealed a tetragonal structure with the P4/mm space group for the B phase, and an orthorhombic structure with the R-3c1-1 space group for the L phase. The dielectric and magnetic properties, as well as the magnetoelectric coupling coefficients (alpha(ME)), vvere measured as a function of frequency. The dielectric constants at 1 kHz were 1560 for the separate B phase and 2970 for the L-B-L sample. Magnetization measurement of the L-B-L pellet showed that the ferromagnetic transition temperature (Tc) was around 304 K. Transverse (41) and longitudinal (aN1) magnetoclectric coupling coefficients were measured for the L-B-L sample aL room temperature, and the maximum values obtained were 055 and 052 mV cm-1 0e-1, respectively.

**Journal Of Magnetism And Magnetic Materials 364, 18-23, 2014. DOI:** 10.1016/j.jmmm.2014.04.014

**[P150-2014] "Measurement of charge multiplicity asymmetry correlations in high-energy nucleus-nucleus collisions at root S-NN=200 GeV"**

Adamczyk, L.; Adkins, J. K.; Agakishiev, G.**; de Souza, R. Derradi*; Takahashi, J.*; Vasconcelos, G. M. S.* ;** et al.
STAR Collaboration

A study is reported of the same-and opposite-sign charge--dependent azimuthal correlations with respect to the event plane in Au+ Au collisions at root(S)(NN) = 200 GeV. The charge multiplicity asymmetries between the up/down and left/right hemispheres relative to the event plane are utilized. The contributions from statistical fluctuations and detector effects were subtracted from the (co-) variance of the observed charge multiplicity asymmetries. In the mid-to most-central collisions, the same- (opposite-) sign pairs are preferentially emitted in back-to-back (aligned on the same-side) directions. The charge separation across the event plane, measured by the difference, Delta, between the like-and unlike-sign up/down-left/right correlations, is largest near the event plane. The difference is found to be proportional to the event-by--event final-state particle ellipticity (via the observed second order harmonic nu(obs)(2)), where Delta = [ 1.3 +/- 1.4( stat) (-1.0)(+4.0)(syst)] x 10(-5) + [3.2 +/- 0.2(stat)(- 0.3)(+0.4)(syst)] x 10(-3)v(2)(obs) for 20- 40% Au + Au collisions. The implications for the proposed chiral magnetic effect are discussed.

**Physical Review C 89[4], 044908, 2014. DOI:** 10.1103/PhysRevC.89.044908

**[P151-2014] "Measurement of charged jet suppression in Pb-Pb collisions at root s(NN)=2.76 TeV"**

Abelev, B.; Adam, J.; Adamova, D.; **Chinellato, D. D.*; Dash, A.*; Takahashi, J.*** ; et al.

A measurement of the transverse momentum spectra of jets in Pb-Pb collisions at root s(NN) = 2.76 TeV is reported. Jets are reconstructed from charged particles using the anti-k(T) jet algorithm with jet resolution parameters R of 0.2 and 0.3 in pseudorapidity vertical bar eta vertical bar < 0.5. The transverse momentum p(T) of charged particles is measured down to 0.15 GeV/c which gives access to the low p(T) fragments of the jet. Jets found in heavy-ion collisions are corrected event--by-event for average background density and on an inclusive basis (via unfolding) for residual background fluctuations and detector effects. A strong suppression of jet production in central events with respect to peripheral events is observed. The suppression is found to be similar to the suppression of charged hadrons, which suggests that substantial energy is radiated at angles larger than the jet resolution parameter R = 0.3 considered in the analysis. The fragmentation bias introduced by selecting jets with a high p(T) leading particle, which rejects jets with a soft fragmentation pattern, has a similar effect on the jet yield for central and peripheral events. The ratio of jet spectra with R = 0.2 and R = 0.3 is found to be similar in Pb-Pb and simulated PYTHIA pp events, indicating no strong broadening of the radial jet structure in the reconstructed jets with R < 0.3.

**Journal Of High Energy Physics [3], 013, 2014. DOI:** 10.1007/JHEP03(2014)013

**[P152-2014] "Measurement of higher-order harmonic azimuthal anisotropy in PbPb collisions at root s(NN)=2.76 TeV"**

Chatrchyan, S.; Khachatryan, V.; Sirunyan, A. M.; **Chinellato, J.*; Tonelli Manganote, E. J.*;** et al.
CMS Collaboration

Measurements are presented by the CMS Collaboration at the Large Hadron Collider (LHC) of the higher-order harmonic coefficients that describe the azimuthal anisotropy of charged particles emitted in root s(NN) = 2.76 TeV PbPb collisions. Expressed in terms of the Fourier components of the azimuthal distribution, the n = 3-6 harmonic coefficients are presented for charged particles as a function of their transverse momentum (0.3 < p(T) < 8.0 GeV/c), collision centrality (0%-70%), and pseudorapidity (|eta| < 2.0). The data are analyzed using the event plane, multiparticle cumulant, and Lee-Yang zeros methods, which provide different sensitivities to initial-state fluctuations. Taken together with earlier LHC measurements of elliptic flow (n = 2), the results on higher--order harmonic coefficients develop a more complete picture of the collective motion in high-energy heavy-ion collisions and shed light on the properties of the produced medium.

**Physical Review C 89[4], UNSP 044906, 2014. DOI:** 10.1103/PhysRevC.89.044906

**[P153-2014] "Measurement of Inclusive W and Z Boson Production Cross Sections in pp Collisions at root s=8 TeV"**

Chatrchyan, S.; Khachatryan, V.; Sirunyan, A. M.; **Chinellato, J.*; Tonelli Manganote, E. J.*** ; et al.

A measurement of total and fiducial inclusive W and Z boson production cross sections in pp collisions at root s = 8 TeV is presented. Electron and muon final states are analyzed in a data sample collected with the CMS detector corresponding to an integrated luminosity of 18.2 +/- 0.5 pb(-1). The measured total inclusive cross sections times branching fractions are sigma(pp -> WX) x B(W -> l upsilon) = 12.21 +/- 0.03(stat) +/- 0.24(syst) +/- 0.32(lum) nb and sigma(pp -> ZX) x B(Z -> l(+) l(-)) = 1.15 +/- 0.01(stat) +/- 0.02(syst) +/- 0.03(lum) nb for the dilepton mass in the range of 60-120 GeV. The measured values agree with next-to-next-to-leading-order QCD cross section calculations. Ratios of cross sections are reported with a precision of 2%. This is the first measurement of inclusive W and Z boson production in proton-proton collisions at root s = 8 TeV.

**Physical Review Letters 112[19], 191802, 2014. DOI:** 10.1103/PhysRevLett.112.191802

**[P154-2014] "Measurement of the W gamma and Z gamma inclusive cross sections in pp collisions at root s=7 TeV and limits on anomalous triple gauge boson couplings"**

Chatrchyan, S.; Khachatryan, V.; Sirunyan, A. M.; **Chinellato, J.*; Tonelli Manganote, E. J.*; et al.**
CMS Collaboration

Measurements of W gamma and Z gamma production in proton--proton collisions at root s = 7 TeV are used to extract limits on anomalous triple gauge couplings. The results are based on data recorded by the CMS experiment at the LHC that correspond to an integrated luminosity of 5.0 fb(-1). The cross sections are measured for photon transverse momenta p(T)(gamma) > 15 GeV, and for separations between photons and final-state charged leptons in the pseudorapidity-azimuthal plane of Delta R(l,gamma) > 0.7 in l nu gamma and ll gamma final states, where l refers either to an electron or a muon. A dilepton invariant mass requirement of m(ll) > 50 GeV is imposed for the Z gamma process. No deviations are observed relative to predictions from the standard model, and limits are set on anomalous WW gamma, ZZ gamma, and Z gamma gamma triple gauge couplings.

**Physical Review D 89[9], 092005, 2014. DOI:** 10.1103/PhysRevD.89.092005

**[P155-2014] "Measurements of the t(t)Overbar charge asymmetry using the dilepton decay channel in pp collisions at root s=7 TeV"**

Chatrchyan, S.; Khachatryan, V.; Sirunyan, A. M.; **Chinellato, J.*; et al.**
CMS Collaboration

The t(t)Overbar charge asymmetry in proton-proton collisions root s = 7TeV is measured using the dilepton decay channel (ee, e mu, or mu mu). The data correspond to a total integrated luminosity of 5.0 fb(-1), collected by the CMS experiment at the LHC. The t(t) Overbar and lepton charge asymmetries, defined as the differences in absolute values of the rapidities between the reconstructed top quarks and antiquarks and of the pseudorapidities between the positive and negative leptons, respectively, are measured to be A(C) = -0.010 +/- 0.017 (stat.) +/- 0.008 (syst.) and A(C)(lep) = 0.009 +/- 0.010 (stat.) +/- 0.006 (syst.). The lepton charge asymmetry is also measured as a function of the invariant mass, rapidity, and transverse momentum of the system. All measurements are consistent with the expectations of the standard model.

**Journal Of High Energy Physics 4[191], 2014. DOI:** 10.1007/JHEP04(2014)191

**[P156-2014] "Metric-signature topological transitions in dispersive metamaterials"**

Reyes-Gomez, E.; Cavalcanti, S. B.; **Oliveira, L. E.***; de Carvalho, C. A. A.

The metric signature topological transitions associated with the propagation of electromagnetic waves in a dispersive metamaterial with frequency-dependent and anisotropic dielectric and magnetic responses are examined in the present work. The components of the reciprocal-space metric tensor depend upon both the electric permittivity and magnetic permeability of the metamaterial, which are taken as Drude-like dispersive models. A thorough study of the frequency dependence of the metric tensor is presented which leads to the possibility of topological transitions of the isofrequency surface determining the wave dynamics inside the medium, to a diverging photonic density of states at some range of frequencies, and to the existence of large wave vectors' modes propagating through the metamaterial.

**Physical Review E 89[3], 033202, 2014. DOI:** 10.1103/PhysRevE.89.033202

**[P157-2014] "Modification of jet shapes in PbPb collisions at root s(NN)=2.76 TeV"**

Chatrchyan, S.; Khachatryan, V.; Sirunyan, A. M.; **Chinellato, J.*; Tonelli Manganote, E. J.***; et al.
CMS Collaboration

The first measurement of jet shapes, defined as the fractional transverse momentum radial distribution, for inclusive jets produced in heavy-ion collisions is presented. Data samples of PbPb and pp collisions, corresponding to integrated luminosities of 150 mu b(-1) and 5.3 pb(-1) respectively, were collected at a nucleon-nucleon centre-of-mass energy of root s(NN) = 2.76 TeV with the CMS detector at the LHC. The jets are reconstructed with the anti-k(T) algorithm with a distance parameter R = 0.3, and the jet shapes are measured for charged particles with transverse momentum P-T > 1 GeV/c. The jet shapes measured in PbPb collisions in different collision centralities are compared to reference distributions based on the pp data. A centrality-dependent modification of the jet shapes is observed in the more central PbPb collisions, indicating a redistribution of the energy inside the jet cone. This measurement provides information about the parton shower mechanism in the hot and dense medium produced in heavy-ion collisions.

**Physics Letters B 730, 243-263, 2014. DOI:** 10.1016/j.physletb.2014.01.042

**[P158-2014] "Multiferroic Behavior of Lead-free AlFeO3 and Mn, Nb Doped Compositions"**

Santos, G. M.; Silva, D. M.; Freitas, V. F.; Dias, G. S.; **Coelho, A. A.***; Pal, M.; Santos, I. A.; Cotica, L. F.; Guo, R.; Bhalla, A. S.

The lead-free AlFeO3-based compounds are attractive multiferroic materials, as those present piezoelectricity and ferrimagnetism at low temperatures. In this work the synthesis and ferroic properties of AlFeO3-based ceramics were investigated. Stoichiometric proportions of the precursors - alpha--Fe2O3 and alpha-Al2O3 - were milled and sintered to obtain AlFeO3 ceramics. Also, AlFeO3 ceramics doped with 2at% of Nb2O5 or MnO2 were sintered in oxygen flow at 1700K. The crystal structure of the samples was studied by X-ray diffraction. The diffractograms were refined by the Rietveld method. The results obtained from refinements showed an orthorhombic symmetry with space group Pna2(1). Dielectric, ferroelectric and magnetic investigations suggested a magnetoelectric coupling between the electric and magnetic orderings at temperatures below similar to 160K for AlFeO3, Al(Fe0.98Nb0.02)O-3 and Al(Fe0.98Mn0.02)O-3, where the compositions show the ferromagnetic and ferroelectric ordering.

**Ferroelectrics 460[1], 108-116, 2014. DOI:** 10.1080/00150193.2014.875332

**[P159-2014] "Nanobiosensor for Diclofop Detection Based on Chemically Modified AFM Probes"**

Bueno, C. C.; Amarante, A. M.; Oliveira, G. S.; Deda, D. K.; **Teschke, O.***; Franca, E. D.; Leite, F. L.

Highly sensitive and selective functional nanobio-breaksensors are being developed because they have significant applications in the sustenance and conservation of natural resources and can be used in projects to identify degraded and contaminated areas (of both soil and water) and as environmental quality indicators. In the present study, a nanobiosensor was developed based on using theoretical models (molecular docking and molecular dynamics simulations) based on biomimicry of the action mechanism of herbicides in plants coupled with atomic force microscopy (AFM) tools. The herbicide molecules were detected at very low concentrations using a unique sensor construction: the AFM probes and the substrate were chemically functionalized to favor covalent bonding and promote molecular flexibility, as well as to achieve reproducible and accurate results.

Computational methods were used to determine the binding energies associated with the enzyme-herbicide interactions, which were compared with experimental results for adhesion forces. The theoretical results showed that the diclofop herbicide could be assembled and attached onto the mica substrate surface and the ACCase enzyme on the AFM probe without damaging the diclofop molecule. The experimental results showed that using a specific agrochemical target molecule was more efficient than using other nonspecific agrochemicals. On average, there was a 90% difference between the values of specific recognition (diclofop) and nonspecific recognition (imazaquin, metsulfuron, and glyphosate). This result validated the selectivity and specificity of the nanobiosensor. The first evidence of diclofop detection by the AFM probe sensors has been presented in this paper.

**IEEE Sensors Journal 14[5], 1467-1475, 2014. DOI:** 10.1109/JSEN.2014.2301997

**[P160-2014] "Nanocomposites with superparamagnetic behavior based on a vegetable oil and magnetite nanoparticles"**

Meiorin, C.; **Muraca, D.*; Pirota, K. R.*;** Aranguren, M. I.; Mosiewicki, M. A.

The direct reaction of unmodified tung oil and styrene initiated by boron trifluoride diethyl etherate allowed obtaining thermoset polymers with valuable properties like shape memory behavior. On the other hand, the addition of magnetite nanoparticles (MNPs) to the tung oil/styrene copolymer was considered, in order to improve/modify its properties. MNPs were synthesized by the method of alkaline coprecipitation, followed by coating with oleic acid in order to hydrophobize their surfaces and make them more compatible with the polymeric matrix. Thus, superparamagnetic polymer nanocomposites were prepared from the inclusion of the MNPs to the cationically copolymerized tung oil (TO) and styrene (St) networks. The morphology, dynamic-mechanical and mechanical properties of the copolymers as well as magnetic behavior were significantly affected by the variation of the concentration of the MNPs.

**European Polymer Journal 53, 90-99, 2014. DOI:** 10.1016/j.eurpolymj.2014.01.018

**[P161-2014] "Near-IR emission in Pr(3+)single doped and tunable near-IR emission in Pr3+/Yb3+ codoped tellurite tungstate glasses for broadband optical amplifiers"**

Belancon, M. P.; Marconi, J. D.; Ando, M. F.; **Barbosa, L. C.***

A study of the broadband near-infrared emission in Pr3+ single doped and Pr3+/Yb3+ codoped tellurite-tungstate glasses for optical amplification is presented. In the Pr3+ single doped samples pumped at 474 nm the emission band at 1480 nm presents a FWHM of similar to 140 nm. The Yb3+ addition produces a FWHM broadening up to 155 nm, achieved through the (1)G(4)-H-3(5) transition. The emission spectra when the codoped sample is pumped at 980 nm shows efficient energy transfer from Yb3+ to Pr3+ resulting in an intense Pr3+ emission around 1330 nm. This shows that changing the pump wavelength it is possible to select the D-1(2)-(1)G(4) or the (1)G(4)-H-3(5) transition, displacing the emission band from similar to 1480 to similar to 1330 nm.

**Optical Materials 36[6], 1020-1026, 2014. DOI:** 10.1016/j.optmat.2014.01.014

**[P162-2014] "On the solid-liquid equilibrium of binary mixtures of fatty alcohols and fatty acids"**

Maximo, G. J.; Carareto, N. D. D.; Costa, M. C.; dos Santos, A. O.; **Cardoso, L. P.***; Krahenbahl, M. A.; Meirelles, A. J. A.

Fatty alcohols and fatty acids are used in the cosmetic, pharmaceutical and food industries as surfactants. They are also considered phase change materials for thermal storage processes. Information on their thermal properties is required for optimizing production processes as well as for improving their industrial and home use. In the present study, the solid-liquid phase diagrams of three binary systems of 1-tetradecanol + dodecanoic acid, 1-hexadecanol + tetradecanoic acid and 1-octadecanol + hexadecanoic acid were determined by differential scanning calorimetry. The phase-transition phenomena were further investigated by optical micrographs and X-ray diffraction patterns. The experimental data showed that the systems present eutectic transitions and some of them exhibit partial solid phase miscibility. The liquid phase activity coefficients were calculated by Margules 2 and 3-suffix and by UNIFAC and UNIFAC-Dortmund methods. The modeling approach resulted in an accurate prediction, with average absolute deviations from experimental data lower than 1.16 K. The values of excess Gibbs free energy present an unusual behavior, with positive deviations at very low alcohol concentrations and negative ones at high concentrations of this component. This occurs due to changes in the H-bonding interactions along the concentration range of the mixture.

**Fluid Phase Equilibria 366, 88-98, 2014. DOI:** 10.1016/j.fluid.2014.01.004

**[P163-2014] "Pattern changes of EEG oscillations and BOLD signals associated with temporal lobe epilepsy as revealed by a working memory task"**

**Ozelo, H. F. B.*; Alessio, A.*; Sercheli, M. S.***; Bilevicius, E.; Pedro, T.; Pereira, F. R. S.; Rondina, J. M.; Damasceno, B. P.; Cendes, F.; **Covolan, R. J. M.***

Background: It is known that the abnormal neural activity in epilepsy may be associated to the reorganization of neural circuits and brain plasticity in various ways. On that basis, we hypothesized that changes in neuronal circuitry due to epilepsy could lead to measurable variations in patterns of both EEG and BOLD signals in patients performing some cognitive task as compared to what would be obtained in normal condition. Thus, the aim of this study was to compare the cerebral areas involved in EEG oscillations versus fMRI signal patterns during a working memory (WM) task in normal controls and patients with refractory mesial temporal lobe epilepsy (MTLE) associated with hippocampal sclerosis (HS). The study included six patients with left MTLE-HS (left-HS group) and seven normal controls (control group) matched to the patients by age and educational level, both groups undergoing a blocked design paradigm based on Sternberg test during separated EEG and fMRI sessions. This test consisted of encoding and maintenance of a variable number of consonant letters on WM. Results: EEG analysis for the encoding period revealed the presence of theta and alpha oscillations in the frontal and parietal areas, respectively. Likewise, fMRI showed the co-occurrence of positive and negative BOLD signals in both brain regions. As for the maintenance period, whereas EEG analysis revealed disappearance of theta oscillation, fMRI showed decrease of positive BOLD in frontal area and increase of negative BOLD in the posterior part of the brain. Conclusions: Generally speaking, these patterns of electrophysiological and hemodynamic signals were observed for both control and left-HS groups. However, the data also revealed remarkable differences between these groups that are consistent with the hypothesis of reorganization of brain circuitry associated with epilepsy.

**BMC Neuroscience 15, 52, 2014. DOI:** 10.1186/1471-2202-15-52

**[P164-2014] "Plaquette valence-bond solid in the square--lattice J(1)-J(2) antiferromagnet Heisenberg model: A bond operator approach"**

**Doretto, R. L.***

We study the plaquette valence-bond solid phase of the spin--1/2J(1)-J(2) antiferromagnet Heisenberg model on the square lattice within the bond-operator theory. We start by considering four S = 1/2 spins on a single plaquette and determine the bond operator representation for the spin operators in terms of singlet, triplet, and quintet boson operators. The formalism is then applied to the J(1)-J(2) model and an effective interacting boson model in terms of singlets and triplets is derived. The effective model is analyzed within the harmonic approximation and the previous results of Zhitomirsky and Ueda [Phys. Rev. B 54, 9007 (1996)] are recovered. By perturbatively including cubic (triplet-triplet-triplet and singlet-triplet-triplet) and quartic interactions, we find that the plaquette valence--bond solid phase is stable within the parameter region 0.34 < J(2)/J(1) < 0.59, which is narrower than the harmonic one. Differently from the harmonic approximation, the excitation gap vanishes at both critical couplings J(2) = 0.34J(1) and J(2) = 0.59J(1). Interestingly, for J(2) < 0.48J(1), the excitation gap corresponds to a singlet-triplet excitation at the Gamma point while, for J(2) > 0.48J(1), it is related to a singlet-singlet excitation at the X = (pi/2,0) point of the tetramerized Brillouin zone.

**Physical Review B 89[10], 104415, 2014. DOI:** 10.1103/PhysRevB.89.104415

**[P165-2014] "Possible superconductivity in multi-layer-graphene by application of a gate voltage"**

Ballestar, A.; Esquinazi, P.; Barzola-Quiquia, J.; Dusari, S.; Bern, F.; **da Silva, R. R.*; Kopelevich, Y.***

The carrier density in tens of nanometers thick graphite samples (multi-layer-graphene, MLG) has been modified by applying a gate voltage (V-g) perpendicular to the graphene planes. Surface potential microscopy shows inhomogeneities in the carrier density (n) in the sample near surface region and under different values of V-g at room temperature. Transport measurements on different MLG samples reveal that under a large enough applied electric field these regions undergo a superconducting-like transition at T less than or similar to 17K. A magnetic field applied parallel or normal to the graphene layers suppresses the transition without changing appreciably the transition temperature.

**Carbon 72, 312-320, 2014. DOI:** 10.1016/j.carbon.2014.02.011

**[P166-2014] "Pressure effects on magnetic pair-breaking in Mn- and Eu-substituted BaFe2As2"**

**Rosa, P. F. S.*; Garitezi, T. M.*; Adriano, C.*;** Grant, T.; Fisk, Z.; **Urbano, R. R.*;** Fernandes, R. M.; **Pagliuso, P. G.***

We report a combined study of hydrostatic pressure (P <= 25 kbar) and chemical substitution on the magnetic pair-breaking effect in Eu- and Mn-substituted BaFe2As2 single crystals. At ambient pressure, both substitutions suppress the superconducting (SC) transition temperature (T-c) of BaFe2-xCoxAs2 samples slightly under the optimally doped region, indicating the presence of a pair-breaking effect. At low pressures, an increase of T-c is observed for all studied compounds followed by an expected decrease at higher pressures. However, in the Eu dilute system, T-c further increases at higher pressure along with a narrowing of the SC transition, suggesting that a pair-breaking mechanism reminiscent of the Eu Kondo single impurity regime is being suppressed by pressure. Furthermore, Electron Spin Resonance (ESR) measurements indicate the presence of Mn2+ and Eu2+ local moments and the microscopic parameters extracted from the ESR analysis reveal that the Abrikosov-Gor'kov expression for magnetic pair-breaking in a conventional sign-preserving superconducting state cannot describe the observed reduction of T-c.

**Journal Of Applied Physics 115[17], 17D702, 2014. DOI:** 10.1063/1.4861577

**[P167-2014] "Probing the radio emission from air showers with polarization measurements"**

Aab, A.; Abreu, P.; Aglietta, M.; **Chinellato, J. A.*; Daniel, B.*; de Mello Junior, W. J. M.*; Dobrigkeit, C.*; Escobar, C. O.*; Fauth, A. C.*; Kemp, E.*; Muller, M. A.*; Selmi-Dei, D. Pakk*; Silva, M. Zimbres*;** et al.
Pierre Auger Collaboration

The emission of radio waves from air showers has been attributed to the so-called geomagnetic emission process. At frequencies around 50 MHz this process leads to coherent radiation which can be observed with rather simple setups. The direction of the electric field induced by this emission process depends only on the local magnetic field vector and on the incoming direction of the air shower. We report on measurements of the electric field vector where, in addition to this geomagnetic component, another component has been observed that cannot be described by the geomagnetic emission process. The data provide strong evidence that the other electric field component is polarized radially with respect to the shower axis, in agreement with predictions made by Askaryan who described radio emission from particle showers due to a negative charge excess in the front of the shower. Our results are compared to calculations which include the radiation mechanism induced by this charge-excess process.

**Physical Review D 89[5], 052002, 2014. DOI:** 10.1103/PhysRevD.89.052002

**[P168-2014] "Quantum dissipation and CP violation in MINOS"**

**Oliveira, R. L. N.*; Guzzo, M. M.*; de Holanda, P. C.***

We use the open quantum systems framework to analyze the MINOS data and perform this analysis considering two different dissipative models. In the first model, the dissipative parameter describes the decoherence effect and in the second, the dissipative parameter describes other dissipative effects including decoherence. With the second model it is possible to study CP violation since we consider Majorana neutrinos. The analysis from the muon neutrino and antineutrino beam assigns different values to all the parameters of the models, but is consistent between them. Assuming that neutrinos are equivalent to antineutrinos, the global analysis presents a nonvanishing Majorana CP phase depending on the energetic parametrization of the dissipative parameter.

**Physical Review D 89[5], 053002, 2014. DOI:** 10.1103/PhysRevD.89.053002

**[P169-2014] "Renormalization group analysis of the gluon mass equation"**

**Aguilar, A. C.***; Binosi, D.; Papavassiliou, J.

We carry out a systematic study of the renormalization properties of the integral equation that determines the momentum evolution of the effective gluon mass in pure Yang--Mills theory, without quark effects taken into account.

A detailed, all-order analysis of the complete kernel appearing in this particular equation, derived in the Landau gauge, reveals that the renormalization procedure may be accomplished through the sole use of ingredients known from the standard perturbative treatment of the theory, with no additional assumptions. However, the subtle interplay of terms operating at the level of the exact equation gets distorted by the approximations usually employed when evaluating the aforementioned kernel. This fact is reflected in the form of the obtained solutions, for which the deviations from the correct behavior are best quantified by resorting to appropriately defined renormalization-group invariant quantities. This analysis, in turn, provides a solid guiding principle for improving the form of the kernel, and furnishes a well-defined criterion for discriminating between various possibilities. Certain renormalization--group inspired Ansatze for the kernel are then proposed, and their numerical implications are explored in detail. One of the solutions obtained fulfills the theoretical expectations to a high degree of accuracy, yielding a gluon mass that is positive definite throughout the entire range of physical momenta, and displays in the ultraviolet the so-called "power-law" running, in agreement with standard arguments based on the operator product expansion. Some of the technical difficulties thwarting a more rigorous determination of the kernel are discussed, and possible future directions are briefly mentioned.

**Physical Review D 89[8], 085032, 2014. DOI:** 10.1103/PhysRevD.89.085032

**[P170-2014] "Search for baryon number violation in top--quark decays"**

Chatrchyan, S.; Khachatryan, V.; Sirunyan, A. M.; **Chinellato, J.*; Tonelli Manganote, E. J.***; et al.
CMS Collaboration

A search for baryon number violation (BNV) in top-quark decays is performed using pp collisions produced by the LHC at root s = 8 TeV. The top-quark decay considered in this search results in one light lepton (muon or electron), two jets, but no neutrino in the final state. Data used for the analysis were collected by the CMS detector and correspond to an integrated luminosity of 19.5 fb(-1). The event selection is optimized for top quarks produced in pairs, with one undergoing the BNV decay and the other the standard model hadronic decay to three jets. No significant excess of events over the expected yield from standard model processes is observed. The upper limits at 95% confidence level on the branching fraction of the BNV top-quark decay are calculated to be 0.0016 and 0.0017 for the muon and the electron channels, respectively. Assuming lepton universality, an upper limit of 0.0015 results from the combination of the two channels. These limits are the first that have been obtained on a BNV process involving the top quark.

**Physics Letters B 731, 173-196, 2014. DOI:** 10.1016/j.physletb.2014.02.033

**[P171-2014] "Search for Top-Quark Partners with Charge 5/3 in the Same-Sign Dilepton Final State"**

Chatrchyan, S.; Khachatryan, V.; Sirunyan, A. M.; **Chinellato, J.*; Tonelli Manganote, E. J.*; Gurtu, A.***; et al.
CMS Collaboration

A search for the production of heavy partners of the top quark with charge 5/3 is performed in events with a pair of same--sign leptons. The data sample corresponds to an integrated luminosity of 19.5 fb(-1) and was collected at root s = 8 TeV by the CMS experiment. No significant excess is observed in the data above the expected background, and the existence of top-quark partners with masses below 800 GeV is excluded at a 95% confidence level, assuming they decay exclusively to tW. This is the first limit on these particles from the LHC, and it is significantly more restrictive than previous limits.

**Physical Review Letters 112[17], UNSP 171801, 2014. DOI:** 10.1103/PhysRevLett.112.171801

**[P172-2014] "Searches for light- and heavy-flavour three-jet resonances in pp collisions at root s=8 TeV"**

Chatrchyan, S.; Khachatryan, V.; Sirunyan, A. M.; **Chinellato, J.*; Tonelli Manganote, E. J.***; et al.
CMS Collaboration

A search for three-jet hadronic resonance production in pp collisions at a centre-of-mass energy of 8 TeV has been conducted by the CMS Collaboration at the LHC with a data sample corresponding to an integrated luminosity of 19.4 fb(-1). The search method is model independent, and events are selected that have high jet multiplicity and large values of jet transverse momenta. The signal models explored assume R-parity--violating supersymmetric gluino pair production and have final states with either only light-flavour jets or both light- and heavy-flavour jets. No significant deviation is found between the selected events and the expected standard model multijet and t (t) over bar background. For a gluino decaying into light-flavour jets, a lower limit of 650 GeV on the gluino mass is set at a 95% confidence level, and for a gluino decaying into one heavy- and two light-flavour jets, gluino masses between 200 and 835 GeV are, for the first time, likewise excluded.

**Physics Letters B 730, 193-214, 2014. DOI:** 10.1016/j.physletb.2014.01.049

**[P173-2014] "Self-organized 2D Ni particles deposited on titanium oxynitride-coated Si sculpted by a low energy ion beam"**

**Morales, M.*; Merlo, R. B.*;** Droppa, R.; **Alvarez, F.***

Self-ordered Ni nanoparticles grown on TiNxOy-coated crystalline silicon previously sculpted by ion beam bombardment are reported. The samples are obtained following a sequential in situ routine deposition procedure. First, crystalline Si is Xe+ bombarded, generating regular patterns. Second, a thin TiNxOy film is grown on the patterned Si substrate. Immediately, nano-sized nickel particles are deposited by ion beam sputtering and temperature-annealed forming a 2D lattice. The self-organized Ni islands are induced by preferential Ni site nucleation on the coated sculpted Si grooves.

**Journal Of Physics D-Applied Physics 47[19], 195303, 2014. DOI:** 10.1088/0022-3727/47/19/195303

**[P174-2014] "Strain-Induced Enhancement of the Electron Energy Relaxation in Strongly Correlated Superconductors"**

Gadermaier, C.; Kabanov, V. V.; **Alexandrov, A. S.*;** Stojchevska, L.; Mertelj, T.; Manzoni, C.; Cerullo, G.; Zhigadlo, N. D.; Karpinski, J.; Cai, Y. Q.; Yao, X.; Toda, Y.; Oda, M.; Sugai, S.; Mihailovic, D.

We use femtosecond optical spectroscopy to systematically measure the primary energy relaxation rate Gamma(1) of photoexcited carriers in cuprate and pnictide superconductors. We find that Gamma(1) increases monotonically with increased negative strain in the crystallographic a axis. Generally, the Bardeen-Shockley deformation potential theorem and, specifically, pressure-induced Raman shifts reported in the literature suggest that increased negative strain enhances electron-phonon coupling,

which implies that the observed direct correspondence between a and Gamma(1) is consistent with the canonical assignment of Gamma(1) to the electron-phonon interaction. The well-known nonmonotonic dependence of the superconducting critical temperature T-c on the a-axis strain is also reflected in a systematic dependence T-c on Gamma(1), with a distinct maximum at intermediate values (similar to 16 ps(-1) at room temperature). The empirical nonmonotonic systematic variation of T-c with the strength of the electron-phonon interaction provides us with unique insight into the role of electron-phonon interaction in relation to the mechanism of high-T-c superconductivity as a crossover phenomenon.

**Physical Review X 4[1], 011056, 2014. DOI:** 10.1103/PhysRevX.4.011056

**[P175-2014] "Structural, electronic and magnetic properties of the series of double perovskites (Ca, Sr)(2-x)LaxFeIrO6"**

Bufaical, L.; **Adriano, C.***; Lora-Serrano, R.; Duque, J. G. S.; Mendonca-Ferreira, L.; Rojas-Ayala, C.; Baggio-Saitovitch, E.; Bittar, E. M.; **Pagliuso, P. G.***

Polycrystalline samples of the series of double perovskites Sr2-xLaxFeIrO6 were synthesized. Their structural, electronic and magnetic properties were investigated by X-ray powder diffraction, Mossbauer spectroscopy, magnetic susceptibility, heat capacity and electrical resistivity experiments. The compounds crystallize in a monoclinic structure and were fitted in space group P2(1)/n, with a significant degree of Fe/Ir cationic disorder. As in Ca2-xLaxFeIrO6 the Sr-based system seems to evolve from an antiferromagnetic ground state for the end members (x=0.0 and x=2.0) to a ferrimagnetic order in the intermediate regions (x similar to 1). Since Mossbauer spectra indicate that Fe valence remains 3+ with doping, this tendency of change in the nature of the microscopic interaction could be attributed to Ir valence changes, induced by La3+ electrical doping. Upon comparing both Ca and Sr series, Sr2-xLaxFeIrO6 is more structurally homogenous and presents higher magnetization and transition temperatures. Magnetic susceptibility measurements at high temperatures on Sr1.2La0.8FeIrO6 indicate a very high ferrimagnetic Curie temperature T-C similar to 700 K. For the Sr2FeIrO6 compound, electrical resistivity experiments under applied pressure suggest that this material might be a Mott insulator.

**Journal Of Solid State Chemistry 212, 23-29, 2014. DOI:** 10.1016/j.jssc.2014.01.007

**[P176-2014] "Study of double parton scattering using W+2--jet events in proton-proton collisions at root s=7 TeV"**

Chatrchyan, S.; Khachatryan, V.; Sirunyan, A. M.; **Chinellato, J.*; Tonelli Manganote, E. J.***; et al.
CMS Collaboration

Double parton scattering is investigated in proton-proton collisions at = 7 TeV where the final state includes a W boson, which decays into a muon and a neutrino, and two jets. The data sample corresponds to an integrated luminosity of 5 fb(-1), collected with the CMS detector at the LHC. Observables sensitive to double parton scattering are investigated after being corrected for detector effects and selection efficiencies. The fraction of W + 2-jet events due to double parton scattering is measured to be 0.055 +/- 0.002 (stat.) +/- 0.014 (syst.). The effective cross section, sigma (eff), characterizing the effective transverse area of hard partonic interactions in collisions between protons is measured to be 20.7 +/- 0.8(stat.) +/- 6.6(syst.)mb.

**Journal Of High Energy Physics 3, 032, 2014. DOI:** 10.1007/JHEP03(2014)032

**[P177-2014] "Tb3+ Luminescence in a-SiNx:H"**

**Bosco, G. F.*; Tessler, L. R.***

Terbium doped hydrogenated amorphous silicon nitride was prepared by reactive RF-sputtering from a silicon target partially covered either with Tb4O7or metallic Tb platelets in a Ar+N2+H2 atmosphere. When the samples have a high enough bandgap they present characteristic Tb3+ luminescence. The luminescence intensity depends on the annealing temperature. For a given smaple, the luminescence intensity under non-resonant excitation is 10 to 20 times smaller than under resonant excitation of Tb3+. The luminescence intensity under resonant excitation slightly increases with temperature, while under non-resonant excitation it decreases with temperature.. These results are interpreted as due to very effective intra-4f radiative recombination processes in Tb3+ in a--SiNx:H. However, the excitation transfer from the matrix is inefficient or our samples are not yet fully optimized for it.

**ECS Transactions 61[5], 141-146, 2014. DOI:** 10.1149/06105.0141ecst

**[P178-2014] "The crucial role of molecular ions in the radial contraction of argon microwave-sustained plasma jets at atmospheric pressure"**

**Ridenti, M. A.*;** Spyrou, N.; **Amorim, J.***

Fourteen ions (Ar+, Ar-2(+), ArH+, H2O+, H+(H2O), H+(H2O)(2), O+, O-2(+), OH+, NO+, N-2(+), N+, Ar-2(+), N-4(+)) were detected, by mass-resolved ion-energy measurements when the discharge was operated at 50W and fluxes of 2.5 and 5.0 slm. The crucial role of three molecular ions (Ar-2(+), ArH+, H2O+) during the radial contraction, from diffuse (r = (750 +/- 50) mu m) to contracted plasma jet (r = (500 +/- 50) mu m), and the relationship between power, gas flow and molecular ions production were pointed out. Ion energy distributions for Ar-2(+), ArH+ and H2O+ exhibit their maxima at high-energies due to low-energy threshold for three-body collision reactions.

**Chemical Physics Letters 595, 83-86, 2014. DOI:** 10.1016/j.cplett.2014.01.050

**[P179-2014] "Theoretical description of the photopyroelectric technique in the slanted detector configuration for thermal diffusivity measurements in fluids"**

Rojas-Trigos, J. B.; Marin, E.; **Mansanares, A. M.***; Cedeno, E.; Juarez-Gracia, G.; Calderon, A.

This work presents an extended description about the theoretical aspects related to the generation of the photopyroelectric signal in a recently proposed wedge-like heat transmission detection configuration, which recreates the well-known Angstrom method (widely used for solid samples) for accurate thermal diffusivity measurement in gases and liquids. The presented model allows for the calculation of the temperature profile detected by the pyroelectric sensor as a function of the excitation beam position, and the study of the influence on it of several parameters, such as spot size, thermal properties of the absorber layer, and geometrical parameters of the measurement cell. Through computer simulations, it has been demonstrated that a narrow temperature distribution is created at the sensor surface, independently of the lateral diffusion of heat taking place at the sample's surface.

**Thermochimica Acta 582, 101-105, 2014. DOI:** 10.1016/j.tca.2014.03.006

**[P180-2014] "Thermal expansion behavior of holes in graphene nanomeshes"**

Mostério, N. C. B.; **Fonseca, A. F.***

The thermal expansion of a hole, in a planar system, follows the same trend as the thermal expansion of the whole system, i.e., the hole expands (contracts) if the material expands (contracts) under thermal excitation. At nanoscale, this phenomenon has not been studied so far. Here, using tools of classical molecular dynamics simulations, we show that graphene nanomeshes (GNMs) behave oppositely: While the whole structure contracts (expands), the nanoholes expand (contract) under thermal excitation. We propose and test a simple mechanism to describe this unexpected behavior in terms of out-of-plane vibrations of the atoms close to and far from the edges of the holes. This mechanism allows us to see that, contrary to usual planar systems, this behavior comes from nonuniform thermal expansion along the structure. Although the thermal expansion of holes in GNMs is contrary to the classical prediction, we verify that the thermal expansion of the whole GNM structure is the same as that of pristine graphene.

**Physical Review B 89, 195437, 2014. DOI:** 10.1103/PhysRevB.89.195437

**[P181-2014]" Thin-disk models in an integrable Weyl-Dirac theory"**

**Vieira, R. S. S.***; Letelier, P. S.

We construct a class of static, axially symmetric solutions representing razor-thin disks of matter in the Integrable Weyl--Dirac theory proposed in Israelit (Found Phys 29: 1303, 1999). The main differences between these solutions and the corresponding general relativistic one are analyzed, focusing on the behavior of physical observables (rotation curves of test particles, density and pressure profiles). We consider the case in which test particles move along Weyl geodesics. The same rotation curve can be obtained from many different solutions of the Weyl-Dirac theory, although some of these solutions present strong qualitative differences with respect to the usual general relativistic model (such as the appearance of a ring-like density profile). In particular, for typical galactic parameters all rotation curves of the Weyl-Dirac model present Keplerian fall-off. As a consequence, we conclude that a more thorough analysis of the problem requires the determination of the gauge function beta on galactic scales, as well as restrictions on the test-particle behavior under the action of the additional geometrical fields introduced by this theory.

**General Relativity And Gravitation 46[1], 1641, 2014. DOI:** 10.1007/s10714-013-1641-7

**[P182-2014] "Transport critical current measurements on a Cu-substituted BaFe2As2 superconductor"**

**Garitezi, T. M.*; Rosa, P. F. S.*; Adriano, C.*; Pagliuso, P. G.***

The critical current density J(c) is a crucial parameter to establish the actual technological potential of a superconducting (SC) material. Furthermore, being proportional to the SC gap parameter, it can reveal important information about the microscopic nature of the SC state in a given material. The FeAs-based class of SC materials has been a focus of intense scientific investigation lately, but direct investigation of J(c) by transport measurements is rather scarce in literature. For these materials, it is very interesting to map J(c) as a function of their distinct SC tuning parameters such as applied pressure and chemical substitution. In this work, detailed investigation of the field, temperature, and pressure dependences of transport critical current density J(c) for Cu-substituted BaFe2As2 single crystals is reported. In this particular material, Cu-substitution has a strong magnetic pair breaking effect. However, with increasing pressure, this sample shows an almost twofold increase of T-c, from 3.2K to 6.9K, which is followed by an increase in J(c). These observations are discussed considering the presence of magnetic pinning centers in the Fe-As plane, which, in principle, could suggest effective routes to increase J(c) in the this class of materials.

**Journal Of Applied Physics 115[17], 17D704, 2014. DOI:** 10.1063/1.4862525

**[P183-2014] "Using spherical wavelets to search for magnetically-induced alignment in the arrival directions of ultra--high energy cosmic rays"**

**Zimbres, M.*;** Batista, R. A.; **Kemp, E.***

Due to the action of the intervening cosmic magnetic fields, ultra--high energy cosmic rays (UHECRs) can be deflected in such a way as to create clustered energy-ordered filamentary structures in the arrival direction of these particles, the so-called multiplets. In this work we propose a new method based on the spherical wavelet transform to identify multiplets in sky maps containing arrival directions of UHECRs. The method is illustrated in simulations with a multiplet embedded in isotropic backgrounds with different numbers of events. The efficiency of the algorithm is assessed through the calculation of Type I and II errors.

**Astroparticle Physics 54, 54-60, 2014. DOI:** 10.1016/j.astropartphys.2013.11.001

**[P184-2014] "Violation of the universal behavior of membranes inside cylindrical tubes at nanoscale"**

**Perim, E.*; Fonseca, A. F.***; Pugno, N. M.; **Galvao, D. S.***

Recently, it was proposed based on classical elasticity theory and experiments at macroscale, that the conformations of sheets inside cylindrical tubes present a universal behavior. A natural question is whether this behavior still holds at nanoscale. Based on molecular-dynamics simulations and analytical modeling for graphene and boron nitride membranes confined inside carbon nanotubes, we show that the class of universality observed at macroscale is violated at nanoscale. The precise origin of these discrepancies is addressed and proven to be related to both surface and atomistic effects.

**EPL 105[5], 56002, 2014. DOI:** 10.1209/0295-5075/105/56002

**[P185-2014] "Voltage controlled electron spin dynamics in resonant tunnelling devices"**

Galeti, H. V. A.; **Brasil, M. J. S. P.***; Galvao, G. Y.; Henini, M.

We investigate the electron spin dynamics in a p-type GaAs/AlAs resonant tunnelling device by measuring the time-and polarized-resolved photoluminescence (PL) from the GaAs quantum well under a high magnetic field (15 T). The voltage dependence of the PL transients have revealed various tunnelling processes with different time constants that give rise to distinct spin--polarized carriers injected into the double-barrier structure.

**Journal Of Physics D-Applied Physics 47[16], 165102, 2014. DOI:** 10.1088/0022-3727/47/16/165102

## Proceedings

**[P186-2014] "Optical characterization, luminescence properties of Er3+ and Er3+/Yb3+ co-doped tellurite glasses for broadband amplification"**

**Meruva, S.*; Carlos, B. L.*; Peres, F. J. J. A.***; Ramachandran, S. (Ed.)

In the present paper, optical absorption and emission spectra and luminescence decay lifetimes of different concentrations, 0.1, 0.3, 0.5, 0.7 and 1.0 mol% of Er3+ and 0.1Er(3+)/0.5Yb(3+) co-doped tellurite glasses (TeO2-Bi2O3-ZnO-Nb2O5) were reported. Judd-Ofelt intensity parameters were determined and used to calculate spontaneous radiative transition probabilities (A(rad)), radiative lifetimes (tau(R)), branching ratios (beta) and stimulated emission cross-sections (sigma(P)) for certain emission transitions. NIR emission at 1.5 mu m and up-conversion spectra of Er3+ and Er3+/Yb3+ co-doped tellurite glasses were measured under excitation wavelength of 980 nm. The absorption, emission and gain cross-sections for I-4(13/2)-> I-4(15/2) transition of Er3+ are determined. The peak emission cross--section of this transition is found to be higher (9.95x10(-21) cm(2)) for 0.1 mol% of Er3+ and lower (6.81x10(-21) cm(2)) for 1.0 mol% of Er3+ doped tellurite glasses, which is comparable to other oxide glasses. The larger peak emission cross-section for lower concentration of Er3+ is due to the high refractive index of glass matrix (2.1547), relation established from Judd--Ofelt theory. The observed full-widths at half maxima (FWHM) for lower and higher concentrations of Er3+ are 64nm and 96 nm respectively. The larger values of FWHM and peak emission cross-sections are potentially useful for optical amplification processes in the design of Erbium doped fiber amplifiers (EDFs). Under 980 nm excitation three strong up-conversion bands were observed at 530nm, 546nm and 665nm. The pump power dependent intensities and mechanisms involved in the up-conversion process have been studied. The luminescence decay profiles for I-4(13/2) level were reported for all glass matrices.

**In: CONFERENCE ON FIBER LASERS XI - TECHNOLOGY, SYSTEMS, AND APPLICATIONS, XI., 2014, San Francisco, Ca. Proceedings... . [S. L.]: Fiber Lasers Xi: Technology, Systems, And Applications, Proceedings of SPIE, 2014. v. 8961, 896132. DOI:** 10.1117/12.2037000

**[P187-2014] "Reviewing recent results from Pierre Auger Observatory"**

**Chinellato, J. A.***
IOP; Auger Collaboration

We present some results from the last three years of operation of the Pierre Auger Observatory. This is a short version of the review talk presented at the 18th International Symposium on Particles, Strings and Cosmology (PASCOS2012). The main topics are related to ultra-high energy cosmic rays and their interactions: energy spectrum, mass composition, neutrino spectrum and hadronic cross section at energies above 10(18) eV.

**In: INTERNATIONAL SYMPOSIUM ON PARTICLES STRINGS AND COSMOLOGY (PASCOS), 18., 2012, Merica, Mexico. Proceedings... . [s. L.]: Journal of Physics Conference Series, 2014. v. 485, UNSP 012033, 1 - 6. DOI:** 10.1088/1742-6596/485/1/012033

**[P188-2014] "Spectroscopic properties of Ho3+, Tm3+ and Ho3+/Tm3+ doped tellurite glasses for fiber laser"**

**Seshadri, M.*; Ferencz Junior, J. A. P.*;** Ratnakaram, Y. C.; **Barbosa, L. C.*;** Ramachandran, S. (Ed.)

Several papers were reported on spectroscopic properties of rare earth doped different host glasses. A complete knowledge of fluorescence properties of rare earth ions in laser materials is necessary to achieve efficient, compact and cheap sources of laser radiation for NIR and mid-IR region. Tellurite glasses are potentially useful for generation of NIR and mid-IR laser radiation due to its special features such as lowest phonon energy (750 cm(-1)) among oxide glasses, reasonably wide transmission region (0.35 - 5 mu m), good glass stability, good rare earth ion solubility, high linear and non-linear refractive index. In the present work, authors prepared Ho3+ and Tm3+ singly doped and Ho3+/Tm3+ co-doped tellurite glasses using conventional melt-quenching method. Spectroscopic measurements and analysis of energy transfer process in Ho3+, Tm3+ and Ho3+/Tm3+ co-doped glasses pumped with 785nm and 451 nm excitation wavelengths have been performed. There are some spectroscopic properties which are important in understanding and modeling of rare earth doped laser materials. Using Judd-Ofelt theory, radiative transition rates (A(rad)), radiative lifetimes (tau(R)) and branching ratios (beta) were estimated for certain excited states of Ho3+ and Tm3+ doped tellurite glasses. The emission cross-sections and gain coefficients have been determined from the absorption spectra of Ho3+ and Tm3+ ions in tellurite glasses. The energy transfer process such as ion cross-relaxation, Tm3+-Ho3+ energy transfer and energy transfer up-conversion were studied and identified to specific candidate for laser operation.

**In: Conference on Fiber Lasers XI - Technology, Systems, and Applications, XI., 2014, San Francisco, Ca. Proceedings... . [S. L.]: Fiber Lasers Xi: Technology, Systems, And Applications, Proceedings of SPIE, 2014. v. 8961, 896139. DOI:** 10.1117/12.2036876

## Correção

**[C076-2014] "Measurement of the t(t)over-bar production cross section in the dilepton channel in pp collisions at root s = 8 TeV (vol 2, 024, 2014)"**

Chatrchyan, S.; Khachatryan, V.; Sirunyan, A. M.; **Chinellato, J.*; Tonelli Manganote, E. J.***; et al.
CMS Collaboration

**Journal Of High Energy Physics [2], 102, 2014. DOI:** 10.1007/JHEP02(2014)102

***Autores do IFGW destacados**

## Defesas de Dissertação - Mestrado

**[D003-2014] "Estudo de defeitos induzidos por implantação/irradiação de íons em Si (001) por difração de raios-X de n-feixes"**
Aluno: Guilherme Calligaris de Andrade
**Data: 20/05/2014**

**[D004-2014] "Uma Introdução à Teoria Quântica de Campos: Quebra Espontânea de Simetria"**
Aluno: Heitor do Amaral Jurkovich
Orientador: Prof. Dr. Marcelo Moraes Guzzo
**Data: 28/05/2014**

**[D005-2014] "Dissipação e Descoerência Quântica em Oscilação de Neutrinos"**
Aluno: Guilherme Balieiro Gomes
Orientador: Prof. Dr. Marcelo Moraes Guzzo
**Data: 29/05/2014**

**[D006-2014] "A Extensão 3-3-1 das Partículas Elementares e suas Aplicações à Cosmologia"**
Aluno: César Peixoto Ferreira
Orientador: Prof. Dr. Marcelo Moraes Guzzo
**Data: 06/06/2014**

**[D007-2014] "Matriz Densidade a Baixas Temperaturas para Sistemas com Interação de Pares"**
Aluno: Bruno Ricardi de Abreu
Orientador: Prof. Dr. Silvio Antonio Sachetto Vitiello
**Data: 30/06/2014**

## Defesas de Teses - Doutorado

**[T010-2014] "Desenvolvimento de um sensor para quantificação de forças em experimentos in situ de microscopia eletrônica"**
Aluno: Vitor Toshiyuki Abrão Oiko
Orientador: Prof. Dr. Daniel Ugarte
**Data: 02/06/2014**

**[T011-2014] "Moléculas Fotônicas para aplicações em Engenharia Espectral e Processamento de Sinais Ópticos"**
Aluno: Luís Alberto Mijam Barêa
Orientador: Prof. Dr. Newton C. Frateschi
**Data: 05/06/2014**

**[T012-2014] "Efeitos quânticos em semimetais de Dirac"**
Aluno: Bruno Cury Camargo
Orientador: Prof. Dr. Iakov Kopelevitch
**Data: 13/06/2014**

**[T013-2014] "Um método espectral eficiente para domínios não-limitados: aplicações a toros auto-gravitantes em torno de buracos negros"**
Aluno: Claiton P. de Oliveira
Orientador: Prof. Dr. Saa
**Data: 16/06/2014**

**[T014-2014] "Caracterização das Medidas de Fundo e Blindagem em Detectores Subterrâneos de Xenônio Líquido"**
Aluno: Bruno S. Rodriguez Miguez
Orientador: Prof. Dr. Pedro C Holanda
**Data: 30/06/2014**

**[T015] "Aspectos Não-Perturbativos e Fenomenológicos do Espalhamento Elástico de Hádrons em Altas e Ultra-Altas Energias"**
Aluno: Daniel Almeida Fagundes
Orientador: Prof. Dr. Marcio Menon
**Data: 03/07/2014**

**Fonte:** Portal IFGW/Pós-graduação - Agenda de Colóquios, Defesas e Seminários.
**Disponível em:** http://portal.ifi.unicamp.br/pos-graduacao

***A partir de janeiro de 2014 o Boletim Abstracta é publicado apenas em versão eletrônica.**
**Acesse o portal Abstracta e faça seu cadastro como leitor, para receber em seu email a notificação de cada novo número publicado:**

**<http://abstracta.ifi.unicamp.br>**


# Abstracta

Instituto de Física
Diretor: Prof. Dr. Newton Cesario Frateschi
Diretor Associado: Prof. Dr. Luís Eduardo Evangelista de Araujo
Universidade Estadual de Campinas - UNICAMP
Cidade Universitária Zeferino Vaz
13083-859 - Campinas - SP - Brasil
e-mail: secdir@ifi.unicamp.br

## Publicação

Biblioteca do Instituto de Física Gleb Wataghin
http://portal.ifi.unicamp.br/biblioteca

Diretora Técnica: Sandra Maria Carlos Cartaxo
Coordenador da Comissão de Biblioteca: Prof. Dr. André Koch Torres de Assis

Elaboração
Maria Graciele Trevisan (Bibliotecária)
contato: infobif@ifi.unicamp.br